Deformable registration of abdominal kilovoltage treatment planning CT and tomotherapy daily megavoltage CT for treatment adaptation

Deshan Yang,[a] Summer R. Chaudhari, S. Murty Goddu, David Pratt, Divya Khullar, Joseph O. Deasy, and Issam El Naqa
Department of Radiation Oncology, Washington University, St. Louis, Missouri 63110

(Received 25 February 2008; revised 18 November 2008; accepted for publication 18 November 2008; published 7 January 2009)

In adaptive radiation therapy the treatment planning kilovoltage CT (kVCT) images need to be registered with daily CT images. Daily megavoltage CT (MVCT) images are generally noisier than the kVCT images. In addition, in the abdomen, low image contrast, differences in bladder filling, differences in bowel, and rectum filling degrade image usefulness and make deformable image registration very difficult. The authors have developed a procedure to overcome these difficulties for better deformable registration between the abdominal kVCT and MVCT images. The procedure includes multiple image preprocessing steps and a two deformable registration steps. The image preprocessing steps include MVCT noise reduction, bowel gas pockets detection and painting, contrast enhancement, and intensity manipulation for critical organs. The first registration step is carried out in the local region of the critical organs (bladder, prostate, and rectum). It requires structure contours of these critical organs on both kVCT and MVCT to obtain good registration accuracy on these critical organs. The second registration step uses the first step results and registers the entire image with less intensive computational requirement. The two-step approach improves the overall computation speed and works together with these image preprocessing steps to achieve better registration accuracy than a regular single step registration. The authors evaluated the procedure on multiple image datasets from prostate cancer patients and gynecological cancer patients. Compared to rigid alignment, the proposed method improves volume matching by over 60% for the critical organs and reduces the prostate landmark registration errors by 50%. © *2009 American Association of Physicists in Medicine*. [DOI: 10.1118/1.3049594]

Key words: deformable image registration, optical flow, megavoltage CT, tomotherapy, adaptive radiation therapy

I. INTRODUCTION

Application of daily CT images into the radiotherapy process is essential for adaptive radiation therapy (ART).[1–3] "ART is a closed-loop radiation treatment process, where the treatment plan can be modified using a systematic feedback of delivered dose information. It intends to improve radiation treatments by monitoring treatment variations and incorporating them into reoptimization of the treatment plan."[1] Deformable image registration between the planning CT images and the daily CT images is very important in ART because it is the basis for voxel by voxel tracking. It is useful for autosegmentation of the anatomical structures, accumulation of delivered dose, etc.[4,5]

Patient's megavoltage CT (MVCT) images are acquired daily on helical tomotherapy unit (Tomotherapy, Madison, WI).[6] The MVCT images are primarily used for patient setup verification[7] in the clinic. They could also be used for daily dose computation.[8] Compared to the treatment planning kilovoltage CT (kVCT) images, the MVCT images are noisier and have lower soft tissue contrast because of the low dose requirement and the high energy x-ray source used for imaging.[6,9,10]

Most applications of MVCT require the MVCT images to be registered to the treatment planning kVCT images.[7] For patient setup verification purposes, the MVCT images are rigidly registered with the kVCT images so that patient's position and treatment couch can be adjusted according to the rigid registration parameters. To achieve targeted adaptation accuracy, the MVCT images need to be registered to the kVCT images using deformable registration in addition to rigid body registration.[5]

Despite the low image quality of the MVCT images, deformable image registration between the MVCT images and the kVCT images is achievable. A recent article by Lu *et al.*[5] used an edge-preserving filter to smooth the MVCT images and then applied a free-form deformable registration algorithm.[11] In general, most single-modality deformable image registration methods might be applicable, but registration accuracy is limited by issues such as intensity mismatching, low image contrast, mismatched objects such as bowel gas and fecal matter in bowel and rectum, and differences in bladder filling status, etc. We believe that these issues may have degraded the registration accuracy in previous efforts on this topic.

One particular issue is related to bladder filling difference and the associated difficulty to accurately register both the bladder and the nearby structures (the prostate and the pelvis bones). To register a full bladder in one image to an empty bladder in another image, the bladder needs to be deformed greatly. Because of the smoothing mechanisms in most de-

formable registration algorithms, other structures near the bladder will also often be greatly deformed if no special precaution is given to these structures. For instance, incorrect deformation of the prostate in a prostate cancer case is clinically not acceptable since the prostate is the treatment target.

Another important issue is related to mismatching objects, such as bowel gas pockets, and different amounts, types, and status of fecal matter in the bowel and the rectum. Because the kVCT images and the MVCT images were acquired on different days, there was no direct correspondence of the gas and the fecal matter in the bowel or in the rectum between these two image sets. These issues constitute great challenges for the intensity-based deformable image registration algorithms. Several methods have been reported in previous studies to mitigate the gas pocket mismatching problems. Foskey *et al.* proposed to combine rigid and deformable registration methods in order to accommodate the regions in the images with no existing correspondence.[12] Davis *et al.* proposed to artificially deflate the gas pockets before the deformable registration.[13] Gao *et al.* proposed to use the rectum contour in the planning CT to find the rectum and the gas pockets in the daily CT and fill the gas pockets with gradient values before the deformable registration.[14]

In this work, we propose a procedure to perform deformable registration for the abdominal MVCT and kVCT images. In Sec. II, we present our solutions for these issues discussed above. Next, we demonstrate results from our proposed method on patients' datasets. Finally, we discuss a few important aspects related to the proposed method before drawing our conclusions.

II. MATERIALS AND METHODS

II.A. CT image acquisition

The CT images were originally acquired for two gynecological (GYN) cancer and three prostate cancer patients who received radiotherapy treatment at Barnes-Jewish Hospital, Saint Louis, MO. Patient images were analyzed retrospectively in this work after receiving IRB approval and the patient's private health information were anonymized accordingly.

The kVCT image of one GYN cancer patient was acquired with a Siemens Emotion Duo 16-slice CT scanner. It consisted of 66 slices and each slice was 512×512 with voxel dimension of $0.976\times0.976\times2.5$ mm^3. The kVCT images of all other patients were acquired with a Philips Brilliance Big Bore 16-slice CT scanner. The numbers of slices in these images were from 85 to 144 and each slice was 512×512 with voxel dimension of $1.17\times1.17\times3$ mm^3.

The daily MVCT images of all patients were acquired by using the onboard Hi-Art II CT scanner of the tomotherapy unit during the course of radiation treatment. Each slice was 512×512 with voxel dimension of $0.754\times0.754\times4$ mm^3. The numbers of slices were different for different patients on different days, ranging from 18 to 60. One kVCT image and two MVCT images per patient were used in this study.

The kVCT images were contoured for treatment planning purposes on Pinnacle version 7.6c treatment planning system (Philips Medical Systems, Cleveland, OH). The critical organs in the MVCT image datasets were also contoured (the bladder, the prostate, and the rectum for prostate patients, and the bladder and the rectum for the GYN patients).

II.B. Image preprocessing

II.B.1. Noise reduction and resampling

To reduce the noise in the MVCT images, we applied a 2D bilateral edge-preserving filter[15] (the half-size of the Gaussian filter window=3 pixels, the spatial domain standard deviation σ_d=1.5 mm, the intensity domain standard deviation σ_r=0.1) following by a 2D Gaussian low-pass filter[16] (σ=0.5 mm) for each MVCT slice. The MVCT images and the kVCT images had different voxel dimensions; we resampled all the image datasets to a uniform voxel dimension $2\times2\times2$ mm^3 using trilinear interpolation.

II.B.2. Rigid alignment

A translation only alignment was performed to align the MVCT image to the corresponding kVCT image in two simple steps: (1) alignment of the centroid on the transverse plane, (2) superior-inferior alignment by extensive searching of the least root-mean-squared error on the difference image for the best matching position. Extensive searching was performed as the images' superior-inferior alignment was changing slice-by-slice. Alignment results were visually examined and quick manual correction was performed if the automatic alignment result was not satisfactory.

II.B.3. Padding and cropping

We designated the MVCT image as the moving image and the kVCT image as the target image for each image pair. This was corresponding to the ART applications of daily dose deformation and accumulation from MVCT to kVCT, and automatic contour propagation from kVCT to MVCT. However, the kVCT image was relatively larger and covered the MVCT image entirely, but our deformable registration algorithm requires that the moving MVCT image should not be smaller than the target kVCT image, therefore: (1) the treatment couch was deleted from the image as the couch region was manually selected in the transverse plane and then set to CT number=0; (2) both the MVCT image and the kVCT image were cropped on the transverse plane to exclude most air space and the deleted couch table; (3) the MVCT image was extended in the transverse plane to same size of the kVCT image; and (4) the kVCT image was cropped in the superior and inferior directions to match the MVCT image. After the padding and cropping processes, the kVCT and the MVCT image datasets had the same dimensions.

II.B.4. Detecting and painting the bowel gas pockets

Our solution for the gas pocket mismatching problem is similar to the detection and filling method by Gao *et al.*[14] Based on the observation that bowels may be filled or have

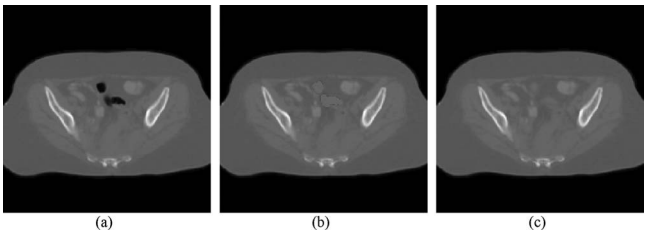

FIG. 1. Examples of bowel gas pocket painting. (a) The original kVCT image. (b) The corresponding MVCT image with bowel gas pockets that are detected and painted. (c) The final MVCT image after gas pocket boundaries are smoothed.

no gas pockets, we detected the gas pockets and painted them with CT number=1060 (the CT number of solid intestines materials). Please note that the CT number used in this article is the Hounsfield number plus 1000. Compared to the previous reported methods,[12–14] our gas pocket painting method does not require additional contour information, or the prior information provided by rigid registration procedures, and does not need to deform the CT images before the deformable registration step. The method works for both the bowel and the rectum. It is comprised of the following steps and the examples are shown in Fig. 1:

(1) *Detection:* For a CT volume I_{original}, all voxels inside the body with CT number below 800 are marked as gas pockets. The value 800 is empirically determined. The result is a binary mask image M_1. All gas pocket voxels in M_1 are set to 1 and all other voxels are set to 0.
(2) *Painting:* Image intensities of all gas pocket voxels are set to 1060. The value 1060 is the average CT number for bowel contents. The painted image is denoted as I_{painted}. A Gaussian low-pass filter with sigma=4 mm is then applied to I_{painted} to get the smoothed image $I_{\text{painted\_smoothed}}$.
(3) *Blurring* the gas pockets and boundaries: M_1 is dilated by 2 voxels to get boundary extended binary mask M_2. A Gaussian low-pass filter with sigma=2 voxel is then applied on M_2 to get M_{2_blurred}. The final result I_{final} is obtained from the interpolation between $I_{\text{painted\_smoothed}}$ and I_{original} using M_{2_blurred} as the per voxel interpolation parameter, as shown in Eq. (1). The purpose of this interpolation step is to achieve a smooth transformation on the boundaries of the gas pockets with the original CT image outside the pockets

$$I_{\text{final}} = I_{\text{original}} \times (1 - M_{2\_\text{blurred}}) + I_{\text{filled\_smoothed}} \times M_{2\_\text{blurred}}. \tag{1}$$

II.B.5. Image contrast enhancement

The image CT number was first limited to the range [700–1300]. Then, the image intensity was normalized from [700–1300] to [0–1] before the actual deformable registration computation. The CT number truncation step and the normalization step together improve the effective image contrast for the soft tissues. This is similar to that the abdominal CT images are viewed with appropriate window level settings to achieve better soft tissue contrast. Such an image contrast enhancement helps to improve registration accuracy in our deformable registration algorithm and improve the convergence speed.

II.C. Deformable registration

II.C.1. The Horn–Schunck algorithm

An in-house implementation of the optical flow deformable registration method proposed by Horn and Schunck[17] was used in this work. Optical flow methods are based on the fundamental principle that the image intensity of corresponding points does not change after an image is deformed (brightness constancy). This intensity constraint of the optical flow is mathematically expressed as:

$$I_1(X - V(X)) = I_2(X), \tag{2}$$

where I_1 is the moving image, I_2 is the target image, X is the image voxel location vector, and V is the optical flow motion field. The constraint in Eq. (2) is insufficient to recover the motion field; therefore, a global smoothness constraint is added to the objective function

$$E = \int_{\Omega} [(\nabla I_1 \cdot V + I_2 - I_1)^2 + \alpha^2(|\nabla u|^2 + |\nabla v|^2 + |\nabla w|^2)] d\Omega, \tag{3}$$

where E is the system energy consisting of a Taylor expansion of Eq. (2) and a smoothness constraint with a regularization parameter α. ∇ is an image gradient operator, Ω is the image domain, u, v, and w are the scalar values of the motion field V in the x, y, and z directions, respectively. This could be numerically solved by a Jacobi or Gauss–Seidal iteration type algorithms.

The multigrid approach and the multiple pass[18] approaches were included in our implementation. With the multigrid approach, registration was carried out sequentially in multiple image resolution stages, from the lower resolution to the higher resolution. With the multiple pass approach, registration was sequentially performed multiple times at each image resolution stage, but with fewer iterations each time. Both approaches helped to increase the convergence speed, the motion capture range and the registration accuracy. After every pass, the motion field was smoothed by a Gaussian low pass filter.[19]

II.C.2. Step one—Registration of bladder and nearby critical structures

In prostate cancer patients, the prostate is the treatment target, and the bladder and the rectum are the critical organs at risk. For treatment adaptation purpose, it is important that all these three organs are accurately registered. We have encountered major registration errors associated with the bladder filling difference between the kVCT image and the MVCT images when attempting to register the images directly. A few registration errors are shown in Fig. 2. Reasons for these errors might be: (1) the registration algorithms can-

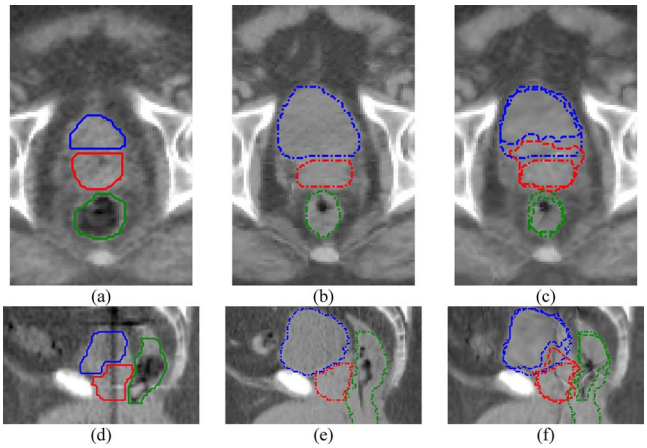

FIG. 2. Registration errors on the critical organs if the images are without painting for these organs. (a) MVCT transverse, (b) kVCT transverse, (c) registered MVCT transverse, (d) MVCT sagittal, (e) kVCT sagittal, (f) registered MVCT sagittal. The bladder, prostate, and the rectum are at the top, middle, and the bottom in (a) to (c), and are at the left, the middle, and the right in (d) to (f), respectively. Solid line, dashed line, and dotted line are for the MV structures, kV structures, and deformed MV structures, respectively. None of these critical organs can be registered satisfactorily in this case.

not distinguish the prostate from the bladder, therefore deformation of the bladder will also cause incorrectly deformation of the prostate; (2) if the boundary of the full bladder is very close to the pelvis bones, deforming the bladder between the full and empty states often causes incorrect deformation of the pelvis bones; and (3) the registration algorithms often confuse the bladder and the nearby bowel contents, and partially register the bladder to these bowel contents.

It is very difficult for image intensity based deformable registration algorithms, including optical flow algorithms, to avoid such registration errors. We therefore propose a more aggressive method. We manipulated the image intensity based on the additional structure contour information for the critical organs in both the kVCT and the MVCT images. Then, we carried out the deformable registration locally. The details of this procedure are as follows:

(1) *Requirement:* Structure contours of the critical organs (prostate, bladder, and rectum) on both the kVCT image and the MVCT images are required. Treatment planning structure contours can be used for the kVCT image. Additional contouring on these organs is needed for the MVCT images. We will discuss other options that would require fewer contours in the discussion section.
(2) *Image cropping:* As the examples in Fig. 2, both images are cropped. The cropped region should be large enough to enclose all critical organs plus some pelvis bones. Pelvis bones are included so that soft tissues near the pelvis bones are correctly registered as the bladder deforms.
(3) *Image intensity manipulation:* For every voxel of the bladder, we updated its image intensity value I as

$$I - I_{\text{avg}} + c \Rightarrow I, \tag{4}$$

where $c=800$, and I_{avg} is the averaged image intensity value of the organ.

For the prostate, we updated the voxel intensity values in a similar way but used $c=1200$ and used I_{avg} of the prostate. For the rectum, we simply overwrote the intensity value for all its voxels to 800. Rectum intensity overwriting was performed only for the slices that rectum was contoured on both the MVCT and the kVCT images. Limiting the slices for the rectum helps to avoid significant mismatching if the rectum has been contoured at a different number of slices in the kVCT images and the MVCT images. Using the constant intensity value for the rectum helps to avoid the intensity mismatching problems caused by the differences of digested food contents in the rectum.

The image intensity manipulations were performed before the image contrast enhancement step. These intensity values 800 and 1200 were empirically selected in order to completely separate the critical organs from each other and from the nearby soft tissues and bony structures.

(4) *Registration:* After intensity manipulations, other parts of the images are not affected. We used the optical flow algorithm to register the cropped and intensity manipulated images. We used two multigrid stages, 50 passes and 30 iterations per pass for the lower-resolution stage, and 10 passes and 5 iterations per pass for the higher-resolution stage. Gaussian low-pass smoothing with sigma=1 mm is applied on the motion field after each pass.
(5) *Extension of the resulting motion field:* Since the registration is computed on the cropped images, the resulting motion field is only defined in the cropped region. We extended it to the entire uncropped volume by repeating the values of the cropping boundary voxels. The repeating values will linearly reduce to 0 at 10 pixels away from the cropping boundaries. Motion vectors on voxels more than 10 pixels away from the cropping boundaries are 0.

II.C.3. Step two—Registration of the entire image

In this step, the MVCT image is deformed by using the extended motion field from the step one and then the deformed MVCT image is registered to the kVCT image. The goals of this step are (1) to register the image outside the cropping region, (2) to fix potential problems caused by the motion field extension procedure at the end of the step one, and (3) to fix possible contouring discrepancy. Since the critical organs have been registered fairly well by the step one, the deformed MVCT image and the kVCT image used in this step are not intensity manipulated. In this way, image registration will be based on intensity matching and will possibly correct the inter- and intraobserver contouring discrepancies.[20] Another option is to use intensity manipu-

lated images in the second registration so that structure contours can be well matched. We will discuss the other options in the discussion section.

For the second registration, two multigrid stages are used with 5 and 2 passes, respectively, for each stage starting from the lower resolution to higher resolution and 10 iterations per pass per stage. A Gaussian low-pass filter with sigma =2 mm is applied on the motion field after every pass. The resulting full volume motion field is then composed with the step-one motion field, which has been extended to full volume, to form the final motion field according to the following equation:

$$V(X) = V_2(X) + V_1[X - V_2(X)], \tag{5}$$

where V_1 is the extended motion field by step one, V_2 is the computed motion fields by step two, and V is the final composite motion field.

After the second registration, the kVCT and the MVCT images are registered not only for the critical organs but also for the entire image volume. The final motion field V represents the voxel mapping from the MVCT image to the kVCT image. It could be used for different applications of treatment adaptation, for example, to deform structure contours from the kVCT to the MVCT for structures not yet contoured on the MVCT, or to deform daily dose computed on the MVCT back to kVCT for dose accumulation purposes.[4,5]

II.D. Evaluation

We visually evaluated the registration results by checking the difference image and the checkerboard images between the deformed MVCT image and the kVCT image. We also measured the landmark correspondence on the prostate cancer case and contour matching on all patients as described below.

For the prostate cancer patients, three golden seed markers (3 mm in length, 1 mm in diameter) were implanted into patients' prostate before treatment for localization purposes. These markers were well distinguishable on both the kVCT images and the MVCT images and therefore identified as landmarks. Absolute registration accuracy was calculated on the coordinates of the landmarks.

For all patients, the volume masks of the critical organs on the MVCT images were deformed using the computed motion fields onto the kVCT image domain and were matched to the corresponding volume masks on the kVCT image. The Dice similarity metric DSC was computed as[21]

$$\mathrm{DSC} = 2 \times \frac{V_{\mathrm{KV}} \cap V_{\mathrm{MV}}}{V_{\mathrm{KV}} + V_{\mathrm{MV}}}, \tag{6}$$

where V_{MV} is the volume of the deformed MVCT structure mask, V_{KV} is the volume of the structure mask defined by the kVCT contour, and $\cap$ is the joint operator.

II.E. Workflow and implementation

The overall workflow is shown in the Fig. 3. We implemented all the described procedures using MATLAB (version 7, Mathworks) on a Dell desktop PC with dual core Xeon 3.0 GHz CPU and 3 GB RAM. For the multigrid approach, we used a Laplacian pyramid filter[22] to perform image half-sampling and used spline interpolation to double-sample the motion fields from a lower resolution stage to the next higher resolution stage. We used a trilinear interpolation method for all volume interpolation. We used α=0.2 in Eq. (3).

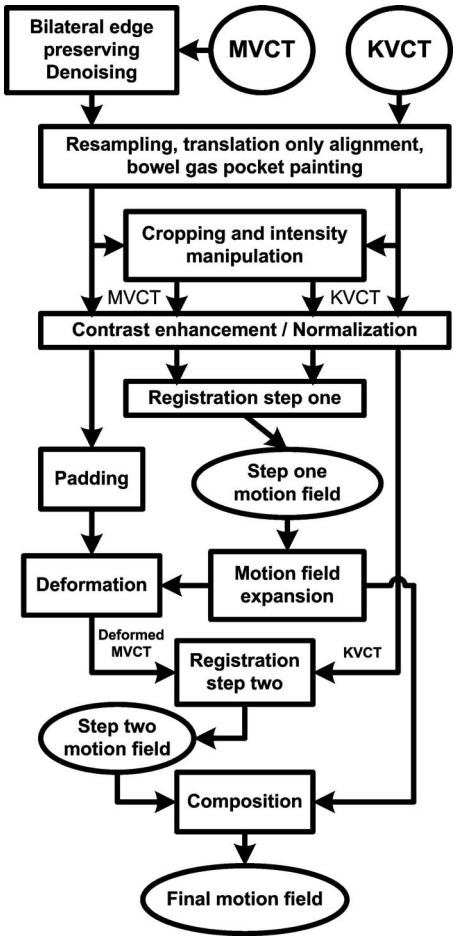

FIG. 3. The overall workflow.

Most procedures are carried out automatically without manual intervention. The cropping step to determine the local region of the critical organs is the only step which needs user interaction. It is possible to automate this step in the future by utilizing treatment planning structure contour information for the critical organs and the pelvis bones.

III. RESULTS AND PERFORMANCE

Figure 4 shows examples of the registration step one. One can see that registration errors were significantly reduced compared to the Fig. 2. The critical organs are not exactly matched because of other constraints applied in the registration computation, including global smoothing, intensity matching of other tissues and structures, etc.

Figure 5 shows examples of the registration step two, which was carried out for the entire images after the step one. It can be seen that both the overall image and the critical organs are generally registered well. The critical organs are

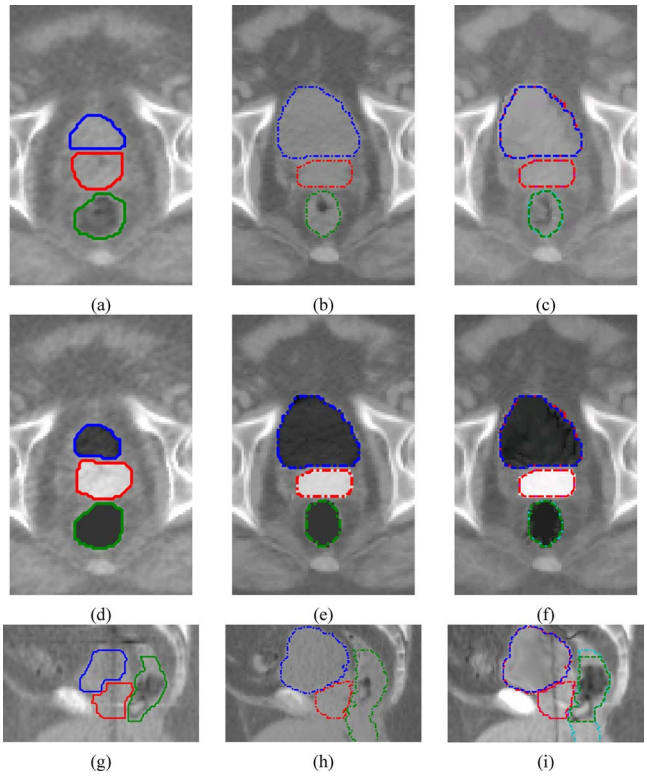

FIG. 4. Step-one deformable registration examples. (a), (d), and (g) are the MVCT images, (b), (e), and (h), are kVCT images; (c), (f), and (i) are the registered MVCT. Critical organs in (d)–(f) are painted. The bladder, the prostate, and the rectum are at the top, the middle, and the right in (g) to (i), respectively. Solid, dashed, and dotted are the line styles for MVCT, kVCT, and deformed MVCT structures, respectively.

slightly less matched than the step-one results because images without intensity manipulation are used in the registration.

Figure 6 shows registration examples for a GYN cancer patient. One can again see that both the overall image and the critical organs are generally registered well.

Table I summarizes the landmark matching results for the prostate cancer cases. The results suggest that the average registration error magnitude is reduced by 66% (from 7.35 to 2.52 mm), compared to rigid alignment results.

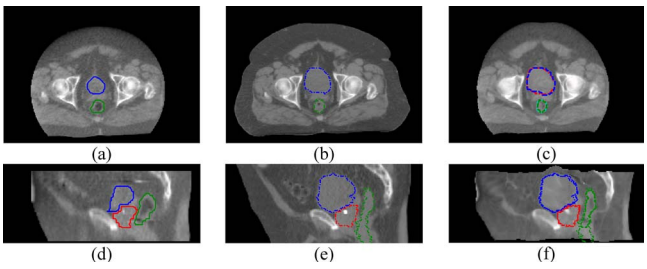

FIG. 5. Step-two deformable registration examples. (a) and (d) are the MVCT images. (b) and (e) are the kVCT images. (c) and (f) are the registered MVCT. The bladder, the prostate, and the rectum are at the top, the middle, and the bottom in (a) to (f), and are at the left, the middle, and the right in (g) to (i), respectively. Solid, dashed, and dotted are the line styles for MVCT, kVCT, and deformed MVCT structures, respectively.

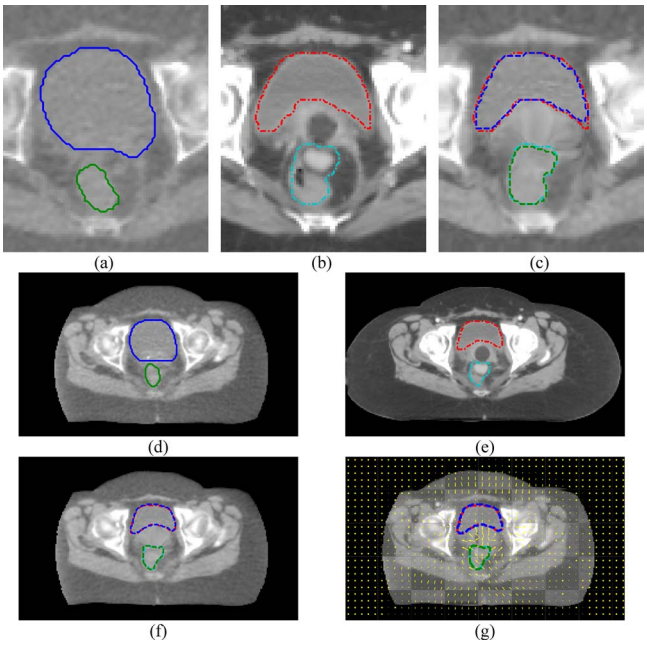

FIG. 6. Deformable registration examples of a GYN cancer patient. (a)–(c) are from the registration step one, (d)–(g) are from the step two. (a) and (d) are the MVCT images, (b) and (e) are the kVCT images, (c) and (f) are the registered MVCT images. (g) is the checkerboard image overlaid with motion vectors. The bladder and the rectum are at the top and the bottom, respectively. Solid, dashed, and dotted are the line styles for MVCT, kVCT, and deformed MVCT structures, respectively.

Table II summarizes the critical organ volume matching results. These results suggest that the proposed procedure is able to significantly improve the volume matching. The average DSC (Dice similarity metric) value is improved by 59% (from the 0.56 to 0.89). Goldberg–Zimring *et al.* suggested that satisfactory volume matching should be 70% or more for adaptive radiotherapy applications.[23] The values in Table II are all higher than 70%, therefore the results are adequately accurate for ART applications according to this criterion.

Table III lists the computation time for the most computationally expensive steps. These values suggest that most computations can be finished within 9 min for a typical kVCT-MVCT pair.

Table IV compares the different registration results on the same prostate cancer patient who has been used in Figs. 2, 4, and 5. Different results are generated by using the MVCT contours for image intensity manipulation in different ways, from not using to fully using the contours on all three critical

TABLE I. Absolute registration errors on implanted landmarks in the prostate cancer case. The listed mean and standard deviation values are computed using all landmarks on six MVCT/kVCT image pairs of the three prostate cancer patients.

Rigid alignment	7.35 ± 3.32 (mm)
Deformable registration after rigid alignment	2.52 ± 1.21 (mm)

TABLE II. Dice similarity metric computed for critical organs before and after deformable registration.

	Rigid alignment			Deformable registration		
Patient No./MVCT No.	Bladder	Rectum[a]	Prostate	Bladder	Rectum[a]	Prostate
Prostate 1/1	0.44	0.72	0.81	0.95	0.77	0.91
Prostate 1/2	0.37	0.61	0.71	0.97	0.78	0.96
Prostate 2/1	0.76	0.62	0.30	0.96	0.81	0.87
Prostate 2/2	0.56	0.58	0.41	0.97	0.83	0.88
Prostate 3/1	0.44	0.58	0.43	0.97	0.81	0.92
Prostate 3/2	0.50	0.62	0.64	0.97	0.79	0.95
GYN 1/1	0.57	0.63	—	0.96	0.77	—
GYN 1/2	0.52	0.56	—	0.93	0.93	—
GYN 2/1	0.40	0.69	—	0.92	0.83	—
GYN 2/2	0.70	0.56	—	0.92	0.78	—
Average	0.52	0.62	0.55	0.95	0.81	0.92

[a]For rectum, the Dice metric is computed only on the slices that rectum was contoured on MVCT images because rectum could have been contoured for different number of slices on MVCT and kVCT.

TABLE III. Computation time of important steps. The results were measured on a Dell Precision desktop PC with 3.00 GHz CPU and 3 GB RAM.

Computation step	Time spent per voxel (10^{-6} s)	Total time spent (s)
Resampling kVCT[a]	1.34	15
Resampling kVCT structure masks	—	11
Resampling MVCT[b]	1.89	5
Resampling MVCT structure masks[e]	—	6
Edge preserving smoothing[b]	32	84
2D Gaussian low pass smoothing[d]	2	8
Gas pocket detecting and painting[a,b]	9.6	17
Step-one registration[c]	263	171
Step-two registration[d]	107	193
Total	118[d]	510

[a]kVCT size was $299\times299\times125$ after resampling.
[b]MVCT size was $193\times193\times71$ after resampling.
[c]Computed on cropped images of size $118\times77\times71$.
[d]Computed on resampled images of size $196\times285\times71$.
[e]Computed only in the regions that structures were defined.

TABLE IV. Comparison of step one registration results on a prostate MVCT and kVCT image pair in different ways of using MVCT structure contours for image intensity manipulation. The Dice similarity values in the rows 1–4 were computed on the corresponding organs on the two images after registration. The values in the row 5 are computed before registration.

		Dice similarity values on organs		
	Intensity manipulation	Bladder	Rectum	Prostate
1	Not applied	0.84	0.76	0.72
2	Bladder only	0.98	0.77	0.87
3	Bladder and rectum	0.98	0.97	0.88
4	Bladder, rectum, and prostate	0.98	0.98	0.99
5	Without registration	0.43	0.74	0.86

organs. One can see that using structure contours would significantly improve the volume matching on these critical organs.

Figure 7 is the same comparison as Table IV but showing the sagittal view of the deformed MVCT image. One can clearly see that using structure contour information to perform image intensity manipulation would help to achieve better registration on the critical organs significantly. The comparison results in Table IV and Fig. 7 will be further discussed in the discussion section.

IV. DISCUSSION

IV.A. Using structure contour information into intensity based deformable registration

We used contouring information of the critical organs to help the image intensity based optical flow algorithm to

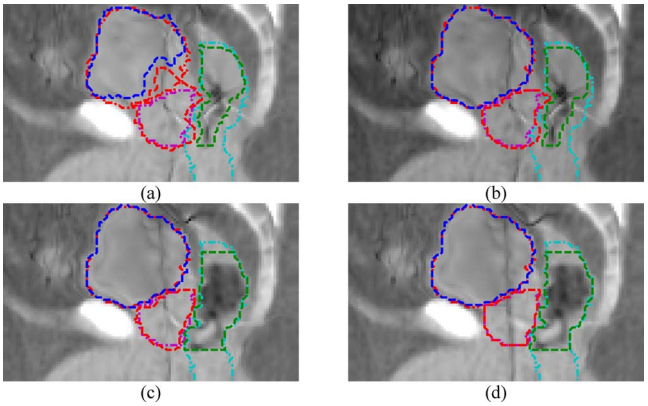

FIG. 7. Comparison of step one registration results for the same patient used in Figs. 2, 4, and 5, and Table IV in different ways of using MVCT structure contours for image intensity manipulation. The images are the deformed MVCT images after registration. The dash-dot lines are the kVCT contours. The dashed lines are the deformed MVCT contours. (a) Without intensity manipulation. (b) Intensity manipulation only on the bladder. (c) Only on the bladder and the rectum. (d) On the bladder, the rectum, and the prostate.

achieve better registration accuracy on these organs. This is a relatively aggressive and atypical approach. The following aspects are worth of further discussion.

Structure information has been widely used in many finite element models (FEMs) based deformable registration algorithms[24,25] which register two images according to physical models and boundary conditions (displacement of structure surfaces). FEM registration algorithms usually ignore the image intensity information which could provide further information for image matching inside and outside the contoured structures. FEM methods and intensity based methods are fundamentally different. Both have their own advantages and disadvantages. An important aspect is that our intensity based method matches both image intensity and structure contours after the intensity manipulation procedure converts the structure contours into additional image intensity information. Our approach may be able to generate more accurate voxel mapping outside the critical structures and on noncontoured objects because image intensity information is better utilized.

IV.B. Limitations and different options to the requirement of MVCT daily contours

Compared to a sole intensity based registration algorithm, an apparent disadvantage of our method is the requirement of structure contours on the daily MVCT images. Without using the structure contour information, it is very difficult for sole intensity based registration algorithms to achieve registration results on these critical structures that are accurate enough for ART applications as seen in the Fig. 2. Compared to our previous best results without using the structure information, we have improved matching on both the critical organs and prostate markers after using the additional structure contour information.

The requirement of the daily critical structure contours on the MVCT could limit the applicability of the proposed method. For treatment adaptation applications, it is desirable that treatment planning contours are automatically propagated to the daily images by using the motion field computed by a deformation image registration algorithm so that the contouring works could be saved. Unfortunately, with the current proposed method, which is based on image intensity matching, it is not possible to generate the motion field as accurate enough for the critical structures without the additional structure information. We have analyzed the reasons in the previous Sec. II C 2.

The proposed method only needs the critical structures contours on MVCT, not other structures. Besides using manual contouring, automatic contouring methods are available. For example, the model-based segmentation in Pinnacle treatment planning system works relatively well for the bladder and the rectum after interactive manual correction according to a previous report[26] and the experience at our institution. However, we have still not seen successful automatic prostate contouring methods based on CT images in the literature. The difficulties in the dedicated automatic contouring algorithms with these critical organs have indirectly explained why a simple intensity based deformable registration algorithm, as applied in this work, has difficulties to have good registration on these organs.

Are there other options to have good registration results without doing labor extensive contouring? For the bladder and the rectum, there are a few possible options according to our experiences: (1) use automatic contouring methods to save manual contouring works; and (2) not use the rectum contours and tolerate additional registration errors on the rectum. It is unlikely that the manual prostate contouring could be saved for the prostate. Fortunately, the prostate usually only covers limited number of slices in the MVCT images.

We have also evaluated another option to use only the contours of the bladder and the rectum, but without the contour of the prostate. In fact, the MVCT and kVCT images could be manually aligned well according to the implanted markers in the prostate. The position of the prostate is always constrained between the bladder and the rectum. After the bladder and the rectum are registered well using the intensity manipulation procedure, the prostate will be registered fairly well. We tested this approach with a few image pairs and we obtained the prostate volume matching from 66% to 88%. The accuracy was not stable and may be not good enough for ART applications. We plan to investigate this option further, to study whether different registration settings or different registration algorithms could work better in this option.

In Table IV and Fig. 7, we have compared the different registration results on one prostate cancer patient, starting from not using to fully using intensity manipulation on the three critical organs. For this particular patient, we can obtain 87%–88% prostate volume overlapping by only using the bladder contour, or using contours of both the bladder and the rectum. One reason for these fairly good results on the prostate was that the prostate was aligned fairly well before registration (86% volume overlapping). For other patients, we have seen worse results. The results in Table IV and Fig. 7 may also suggest that the bladder contour is very necessary. Without using it, deformation of the bladder may also incorrectly deform the prostate because these two organs are next to each other and cannot be easily separated based only on the image intensity information.

IV.C. Why two deformable registration steps

As mentioned in earlier sections, step one is optimized to give good registration for local region of the critical organs, and step two is optimized to perform a typical intensity-based registration for all the other tissues (bones, muscles, body skin surfaces, etc.) and to correct minor registration errors that could have been caused by the step one. The two-step approach is designed for the overall registration accuracy and computation efficiency. It would be difficult to merge the two steps into a single step and still meet the registration requirements of local accuracy (for the critical organs), global accuracy, global smoothness, and computational efficiency. Local accuracy versus global smoothness and accuracy versus computational efficiency could be conflicting requirements. It is easier to achieve such conflicting

goals by using the two-step approach. In a single step approach, these conflicting goals may be traded, could require more computation, or result in less registration accuracy that could be inadequate for ART applications.

Accuracy of the structure contours is an issue and would affect the registration performance. Contouring errors will admittedly affect the registration accuracy for the registration step one. We do not apply the image intensity manipulation procedure for the registration step two therefore the second registration is based on image intensity matching only (after the critical organs are well registered by the step one). With such a choice we hope that inter- and intraobserver contouring discrepancies[20] could be automatically corrected. This choice also makes the registration step one as the preliminary step to align the critical organs, and the step two as the final decisive step. One issue is that the structure contours will be less well matched after the second step two. Another possible option is to use the intensity manipulated images into the second step. In this way, the structure contours will be better matched after the step two. We are planning to perform further study to compare the two options, and to study if the contouring discrepancies could be corrected by using intensity matching. In a single step approach, there will be no choice but to use intensity manipulated image in the registration, therefore the possible contouring discrepancy correction in the second step will be not available.

IV.D. Image preprocessing steps

The procedures reported in this study are configured to give better results for the critical organs and to compromise the MVCT image quality issues. Many of these procedures, for example, contrast enhancement, critical organ image intensity manipulation, bowel gas pocket painting, etc., are also applicable for other abdominal image deformable registration applications, e.g., kVCT to kVCT, and kVCT to CBCT. For the daily CBCT images, we expect that registration accuracy may be better because the CBCT images have better soft tissue contrast.

IV.E. Problems of evaluation

Because there is lack of the ground truth, the absolute accuracy of the computed motion fields cannot be exactly determined. Although we have evaluated our procedure using landmarks and contour matching, these results need to be cautiously interpreted because of the associated uncertainties. The implanted golden seeds may migrate slightly within the prostate from day to day. Furthermore, the accuracy of the landmark positions is limited by the image resolution (the MVCT image has slice thickness of 4 mm). The contours were drawn on the kVCT and MVCT images separately by different physicians. There is reported interobserver variability that should be accounted for. Moreover, the critical structures—the rectum, the prostate, and the bladder, are generally too difficult to be contoured accurately, especially on the MVCT images. Because we have used the structure contours in the registration computation, our contour matching results may be interpreted in terms of the ability to warp these contoured structures into each other rather than in terms of absolute registration accuracy of these structures.

Phantom studies may be necessary to further quantify the results of the proposed techniques but such study would require construction of the deformable phantoms with ability to simulate different MVCT image tissues, which may not be a straightforward task and will be the subject of future research.

V. CONCLUSION

In this work, we proposed a two-step procedure to perform deformable registration for the treatment planning kVCT images and the daily MVCT images. In step one, we manipulated the image intensity of the critical organs then performed registration in the local region of the critical organs in order to have good registration on the critical organs. In step two, we used step one results and continuously registered the entire images. In this way, we obtained better registration accuracy for the entire image than a regular single step registration. The proposed procedure could be useful for adaptive radiotherapy applications for prostate cancer and GYN cancer patients.

ACKNOWLEDGMENTS

This research was partially supported by a grant from the American Cancer Society IRG-58-010-50 and Tomotherapy, Inc.

[a]Electronic mail: dyang@radonc.wustl.edu

[1]D. Yan, F. Vicini, J. Wong, and A. Martinez, "Adaptive radiation therapy," Phys. Med. Biol. **42**, 123–132 (1997).
[2]D. Yan, J. Wong, F. Vicini, J. Michalski, C. Pan, A. Frazier, E. Horwitz, and A. Martinez, "Adaptive modification of treatment planning to minimize the deleterious effects of treatment setup errors," Int. J. Radiat. Oncol., Biol., Phys. **38**, 197–206 (1997).
[3]T. R. Mackie, J. Kapatoes, K. Ruchala, W. Lu, C. Wu, G. Olivera, L. Forrest, W. Tome, J. Welsh, R. Jeraj, P. Harari, P. Reckwerdt, B. Paliwal, M. Ritter, H. Keller, J. Fowler, and M. Mehta, "Image guidance for precise conformal radiotherapy," Int. J. Radiat. Oncol., Biol., Phys. **56**, 89–105 (2003).
[4]D. Yang, H. Li, D. A. Low, J. O. Deasy, and I. El Naqa, "A fast inverse consistent deformable image registration method based on symmetric optical flow computation," Phys. Med. Biol. **53**, 6143–6165 (2008).
[5]W. Lu, G. H. Olivera, Q. Chen, K. J. Ruchala, J. Haimerl, S. L. Meeks, K. M. Langen, and P. A. Kupelian, "Deformable registration of the planning image (kVCT) and the daily images (MVCT) for adaptive radiation therapy," Phys. Med. Biol. **51**, 4357–4374 (2006).
[6]K. J. Ruchala, G. H. Olivera, E. A. Schloesser, and T. R. Mackie, "Megavoltage CT on a tomotherapy system," Phys. Med. Biol. **44**, 2597–2621 (1999).
[7]L. J. Forrest, T. R. Mackie, K. Ruchala, M. Turek, J. Kapatoes, H. Jaradat, S. Hui, J. Balog, D. M. Vail, and M. P. Mehta, "The utility of megavoltage computed tomography images from a helical tomotherapy system for setup verification purposes," Int. J. Radiat. Oncol., Biol., Phys. **60**, 1639–1644 (2004).
[8]K. M. Langen, S. L. Meeks, D. O. Poole, T. H. Wagner, T. R. Willoughby, P. A. Kupelian, K. J. Ruchala, J. Haimerl, and G. H. Olivera, "The use of megavoltage CT (MVCT) images for dose recomputations," Phys. Med. Biol. **50**, 4259–4276 (2005).
[9]K. J. Ruchala, G. H. Olivera, J. M. Kapatoes, E. A. Schloesser, P. J. Reckwerdt, and T. R. Mackie, "Megavoltage CT image reconstruction during tomotherapy treatments," Phys. Med. Biol. **45**, 3545–3562 (2000).
[10]S. L. Meeks, J. F. Harmon, Jr., K. M. Langen, T. R. Willoughby, T. H. Wagner, and P. A. Kupelian, "Performance characterization of megavolt-

age computed tomography imaging on a helical tomotherapy unit," Med. Phys. **32**, 2673–2681 (2005).
[11]W. Lu, M. L. Chen, G. H. Olivera, K. J. Ruchala, and T. R. Mackie, "Fast free-form deformable registration via calculus of variations," Phys. Med. Biol. **49**, 3067–3087 (2004).
[12]M. Foskey, B. Davis, L. Goyal, S. Chang, E. Chaney, N. Strehl, S. Tomei, J. Rosenman, and S. Joshi, "Large deformation three-dimensional image registration in image-guided radiation therapy," Phys. Med. Biol. **50**, 5869–5892 (2005).
[13]B. Davis, D. Prigent, J. Bechtel, J. Rosenman, D. M. Lovelock, and S. Joshi, "Accommodating bowel gas in large deformation image registration for adaptive radiation therapy of the prostate," presented at the AAPM, Pittsburgh, Pennsyvania, 2004 (unpublished).
[14]S. Gao, L. Zhang, H. Wang, R. D. Crevoisier, D. D. Kuban, R. Mohan, and L. Dong, "A deformable image registration method to handle distended rectums in prostate cancer radiotherapy," Med. Phys. **33**, 3304–3312 (2006).
[15]C. Tomasi and R. Manduchi, "Bilateral filtering for gray and color images," Int. Conf. Comput Vision, 1998, pp. 839–846.
[16]R. C. Gonzalez and R. E. Woods, *Digital Image Processing*, 2nd ed. (Prentice Hall, Englewood Cliffs, NJ, 2002).
[17]B. K. P. Horn and B. G. Schunck, "Determining optical flow," Artif. Intell. **17**, 185–203 (1981).
[18]S.-L. Iu and Y.-T. Lin, "Re-examining the optical flow constraint—A new optical flow algorithm with outlier rejection," Int. Conf. Image. Proc. **3**, 727–731 (1999).
[19]J. P. Thirion, "Image matching as a diffusion process: An analogy with Maxwell's demons," Med. Image Anal. **2**, 243–260 (1998).
[20]C. Fiorino, M. Reni, A. Bolognesi, G. M. Cattaneo, and R. Calandrino, "Intra- and inter-observer variability in contouring prostate and seminal vesicles: implications for conformal treatment planning," Radiother. Oncol. **47**, 285–292 (1998).
[21]L. R. Dice, "Measures of the amount of ecologic association between species," Ecology **26**, 297–302 (1945).
[22]P. J. Burt and E. H. Adelson, "The Laplacian pyramid as a compact image code," IEEE Trans. Commun. **31**, 532–540 (1983).
[23]D. Goldberg-Zimring, I.-F. Talos, J. G. Bhagwat, S. J. Haker, P. M. Black, and K. H. Zou, "Statistical validation of brain tumor shape approximation via spherical harmonics for image-guided neurosurgery," Acad. Radiol. **12**, 459–466 (2005).
[24]X. Li, V. Akila, J. S. Alexandra, H. Steven, M. T. Clare, M. C. Lee, and A. C. Robert, "Deformable structure registration of bladder through surface mapping," Med. Phys. **33**, 1848–1856 (2006).
[25]J. R. Crouch, S. M. Pizer, E. L. Chaney, Y.-C. Hu, G. S. Mageras, and M. Zaider, "Automated finite-element analysis for deformable registration of prostate images," IEEE Trans. Med. Imaging **26**, 1379–1390 (2007).
[26]V. Pekar, T. R. McNutt, and M. R. Kaus, "Automated model-based organ delineation for radiotherapy planning in prostatic region," Int. J. Radiat. Oncol., Biol., Phys. **60**, 973–980 (2004).